

# Real-Time Stochastic Optimal Control for Multi-agent Quadrotor Swarms

Vicenç Gómez<sup>1,2</sup>, Sep Thijssen<sup>2</sup>, Hilbert J. Kappen<sup>2</sup>, Stephen Hailes<sup>3</sup>, and Andrew Symington<sup>3</sup>

<sup>1</sup>Department of Information and Communication Technologies

Universitat Pompeu Fabra, Barcelona, Spain

<sup>2</sup>Donders Institute for Brain, Cognition and Behaviour

Radboud University Nijmegen, the Netherlands

<sup>3</sup>Department of Computer Science

University College London, United Kingdom

November 22, 2014

## Abstract

This paper presents a novel method for controlling swarms of unmanned aerial vehicles using Stochastic Optimal Control (SOC) theory. The approach consists of a centralized high-level controller that computes optimal state trajectories as velocity sequences, and a platform-specific low-level controller which ensures that these velocity sequences are met. The high-level control task is expressed as a centralized Path Integral control problem, for which optimal control computation corresponds to a probabilistic inference problem that can be solved by efficient sampling methods. Through simulation we show that our SOC approach (a) has significant benefits compared to deterministic control and other SOC methods in multi-modal problems with noise-dependent optimal solutions, (b) is capable of controlling a large number of platforms in real-time, and (c) yields collective emergent behavior in the form of flight formations. Finally, we show that our approach works for real platforms, by controlling a swarm of three quadrotors.

## 1 Introduction

The recent surge in autonomous Unmanned Aerial Vehicle (UAV) research has been driven by the ease with which platforms can now be acquired, evolving legislation that regulates their use, and the broad range of applications enabled by both individual platforms and cooperative swarms. Example applications include automated delivery systems, monitoring and surveillance, target tracking, disaster management and navigation in areas inaccessible to humans.

Quadrotors are a natural choice for an experimental platform, as they provide a safe, highly-agile and inexpensive means by which to evaluate UAV controllers. Figure 1 shows a 3D model of one such quadrotor, the *Ascending Technologies Pelican*. Quadrotors have non-linear dynamics and are naturally unstable, making control a non-trivial problem.

Stochastic optimal control (SOC) provides a promising theoretical framework for achieving autonomous control of quadrotor swarms. In contrast to deterministic control, SOC directly captures the uncertainty typically present in noisy environments and leads to solutions that qualitatively depend on the level of uncertainty [1]. However, with the exception of the simple Linear Quadratic Gaussian case, for which a closed form solution exists, solving the SOC problem requires solving the Hamilton Jacobi Bellman (HJB) equations. These equations are intractable in the general case, and so the SOC problem remains an open challenge.

In such a complex setting, a hierarchical approach is usually taken and the control problem is reduced to follow a state-trajectory (or a set of way points) designed by hand or computed offline using trajectory

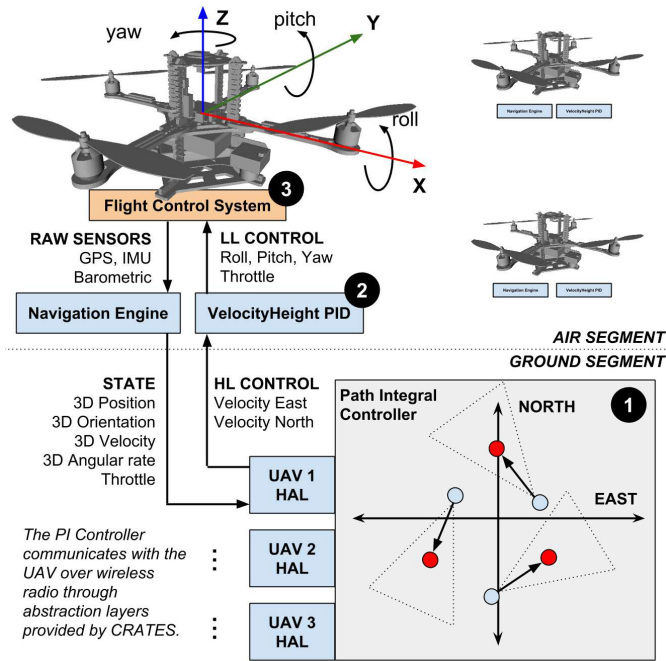


Figure 1: Control hierarchy: The PI controller (1) calculates target velocities/heights for each quadrotor. These are converted to roll, pitch, throttle and yaw rates by a platform-specific VelocityHeight PID controller (2). This control is in turn passed to the platform’s flight control system (3), and converted to relative motor speed changes.

planning algorithms [2]. While the planning step typically involves a low-dimensional state representation, the control methods use a detailed complex state representation of the UAV. Examples of control methods for trajectory tracking are the Proportional Integral Derivative or the Linear-Quadratic regulator.

A generic class of SOC problems was introduced in [1, 3] for which the controls and the cost function are restricted in a way that makes the HJB equation linear and therefore more efficiently solvable. This class of problems is known as Path Integral (PI) control, linearly-solvable controlled diffusions or Kullback-Leibler control, and it has led to successful robotic applications, e.g. [4, 5, 6].

A particularly interesting feature of this class of problems is that the computation of optimal control is an inference problem with a solution given in terms of the passive dynamics. In a multi-agent system, where the agents follow independent passive dynamics, such a feature can be exploited using approximate inference methods such as variational approximations or belief propagation [7, 8].

In this paper, we show how PI control can be used to control a swarm of quadrotors. Rather than using offline path planning to compute a desired state trajectory, we combine periodic re-planning (as it is done in model predictive control) with efficient importance sampling. Our hierarchical approach models at a high-level each quadrotor as a point mass that follows simple double integrator dynamics. Low-level control is achieved using a standard Proportional Integral Derivative (PID) velocity controller that interacts with a real or simulated flight control system. To the best of our knowledge this is the first real-time implementation of PI control on an actual multi-agent system.

In the next section we describe related work. We introduce our approach in Section 3 and show results on three different scenarios in Section 4. Section 5 concludes this paper.

## 2 Related work

Stochastic optimal control is mostly used for UAV control in its simplest form, assuming a linear model perturbed by additive Gaussian noise and subject to quadratic costs (LQG), e.g. [9]. While LQG can successfully perform simple actions like hovering, executing more complex actions requires considering additional corrections for aerodynamic effects such as induced power or blade flapping [10]. These

approaches are mainly designed for accurate trajectory control and assume a given desired state trajectory that the controller transforms into motor commands. The reader is referred to [2] for a recent overview on tracking control methods for general UAVs.

Model Predictive Control (MPC) has been used to optimize trajectories in multi-agent UAV systems [11]. MPC typically employs a detailed model of the UAV and involves solving an optimal control problem at time  $t$  and state  $x(t)$  over a future horizon of a fixed number of time-steps. The first optimal move  $u^*(t)$  is then applied and the rest of the optimal sequence is discarded. The process is repeated again at time  $t + 1$  (replanning). A quadratic cost function is typically used, but other more complex functions exist.

MPC has mostly been used in indoor scenarios, where high-precision motion capture systems are available. For instance, in [12] authors generate smooth trajectories through known 3-D environments satisfying specifications on intermediate waypoints and show remarkable success controlling a team of 20 quadrotors. Trajectory optimization is translated to a linear integer quadratic program problem with additional constraints for collision avoidance, which can be solved efficiently in real-time. Examples that follow a similar methodology can be found in [13, 14]. Similarly to our approach, these methods use a simplified model of dynamics, either using the 3-D position and yaw angle [12, 13] or the position and velocities as in [14]. However, these approaches are inherently deterministic and express the optimal control problem as a quadratic problem. In our case, we solve an inference problem by sampling and we do not require intermediate trajectory waypoints.

In outdoor scenarios motion capture is not possible, and the lower-accuracy Global Positioning System is used instead. Existing control approaches are typically either based on Reynolds flocking [15] or flight formation [16]. In Reynolds flocking each agent is considered as a point mass that obeys simple and distributed rules: separate oneself from neighbors, align oneself with the average heading of neighbors, and steer towards neighborhood centroid to keep cohesion. Flight formation control is typically modeled using graphs, where every node in a graph is an agent that can exchange information with all or several agents. Velocity and/or position coordination is usually achieved using consensus algorithms.

The recent work of [17] is perhaps the most representative work in Reynolds flocking. They present a multi-agent flock of quadrotors that performs stable outdoor flight with up to ten flying agents. They showed collective target tracking achieving different stable formation flights in real platforms under noisy and windy environments. Similarly to our approach, the low-level controller takes the form of a Velocity PID controller. However, whereas their model is based on velocities (self-propelled flocking model), we use a double integrator where the control is defined as acceleration. Similar approaches have been taken in [18] for a flock of ten fixed-wing UAVs and in [19] for a group of five quadrotors. Contrary to our approach, these works are not based on SOC.

In [20] a consensus based formation protocol is presented for quadrotors to achieve a desired time-varying formation. They use double integrator dynamics, as in our work. However, the formation needs to be specified in advance and their approach is based on transforming the flight formation problem into a consensus problem and not based on SOC.

The work that shares most similarities with our approach is [21]. Authors derive a stochastic optimal control formulation of the flocking problem for fixed-wings UAVs. They take a leader-follower strategy, where the leader follows an arbitrary (predefined) policy that is learned offline and define the immediate cost as a function of the distance and heading with respect to the leader. Their method is demonstrated outdoors with 3 fixed-wing UAVs in a distributed sensing task. As in this paper, they formulate a SOC problem and perform MPC. However, in our case we do not restrict to a leader-follower setup and consider a more general class of SOC problems which can include coordination and cooperation problems.

### 3 Path Integral Control

A brief review of Path Integral control theory is given below. This is followed by a description of the methodology used to achieve PI control of multi-agent UAV systems.

#### 3.1 Linearly-solvable controlled diffusions

PI control considers continuous time stochastic control problems, where the dynamics and cost are respectively linear and quadratic in the control input, but arbitrary in the state. More precisely, consider the

following stochastic differential equation of the state vector  $\mathbf{x} \in \mathbb{R}^n$  under controls  $\mathbf{u} \in \mathbb{R}^m$

$$d\mathbf{x} = \mathbf{f}(\mathbf{x})dt + \mathbf{G}(\mathbf{x})(\mathbf{u}dt + d\boldsymbol{\xi}), \quad (1)$$

where  $\boldsymbol{\xi}$  is  $m$ -dimensional Wiener noise with covariance  $\Sigma_u \in \mathbb{R}^{m \times m}$  and  $\mathbf{f}(\mathbf{x}) \in \mathbb{R}^n$  and  $\mathbf{G}(\mathbf{x}) \in \mathbb{R}^{n \times m}$  are arbitrary functions,  $\mathbf{f}$  is the drift in the uncontrolled dynamics (including gravity, Coriolis and centripetal forces), and  $\mathbf{G}$  describes the effect of the control  $\mathbf{u}$  into the state vector  $\mathbf{x}$ .

A realization  $\boldsymbol{\tau} = \mathbf{x}_{0:dt:T}$  of the above equation is called a (random) path. In order to describe a control problem we define the cost that is attributed to a path by

$$S(\boldsymbol{\tau}|\mathbf{x}_0, \mathbf{u}) = \sum_{t=0:dt:T} r_t(\mathbf{x}_t)dt + \mathbf{u}_t^\top \Sigma_u^{-1} \left( \frac{1}{2} \mathbf{u}_t dt + d\boldsymbol{\xi}_t \right), \quad (2)$$

where  $r_t$  is an arbitrary function of the state. The PI control problem is to minimize the expected cost w.r.t. control

$$\mathbf{u}^* = \arg \min_{\mathbf{u}} \mathbb{E}[S(\boldsymbol{\tau}|\mathbf{x}_0, \mathbf{u})].$$

A log transformation yields a linearization of the control problem. The Feynman-Kac Formula expresses optimal control in terms of a path integral, which can be interpreted as taking the expectation under the optimal path distribution.

Let  $p(\boldsymbol{\tau}|\mathbf{x}_0, \mathbf{u})$  denote the probability of a (sub-optimal) path under Eq. (1), then the optimal unnormalized path distribution and expected optimal control are given by

$$p^*(\boldsymbol{\tau}|\mathbf{x}_0) \propto p(\boldsymbol{\tau}|\mathbf{x}_0, \mathbf{u}) \exp(-S(\boldsymbol{\tau}|\mathbf{x}_0, \mathbf{u})), \quad (3)$$

$$\langle \mathbf{u}_t^*(\mathbf{x}_0) \rangle = \langle \mathbf{u}_t + (\boldsymbol{\xi}_{t+dt} - \boldsymbol{\xi}_t)/dt \rangle, \quad (4)$$

where  $\langle \cdot \rangle$  denotes expectation over paths distributed by  $p^*$ .

Eq. (4) permits optimal control to be calculated by probabilistic inference methods, e.g., Monte Carlo. An interesting fact is that Eqs. (3, 4) hold for all controls  $\mathbf{u}$ . In particular,  $\mathbf{u}$  can be chosen to reduce the variance in the Monte Carlo computation of  $\langle \mathbf{u}_t^*(\mathbf{x}_0) \rangle$  which amounts to importance sampling. This technique can drastically improve the sampling efficiency, which is crucial in high dimensional systems.

### 3.2 PI Control for multi UAV systems

Two main limitations prevent the direct application of PI control to real systems: first, note that Eq. (4) yields the optimal control for all times  $t$  averaged over states. The result is therefore an open-loop controller that neglects the state-dependence of the control beyond the initial state. Second, current sampling procedures are inefficient and do not scale well to high dimensional systems. Addressing these issues is the focus of current research [22, 23, 24].

In this work, we circumvent these issues by using real-time Model Predictive Control and importance sampling. Rather than considering a full, high-dimensional, non-linear system, our multi-agent system will be modeled as a 2D point-mass system that follows double integrator dynamics. The choice of 2D is not a fundamental limitation of the method, as long as double-integrator dynamics is used. Having a reduced dimension and simplified model dynamics facilitates inference at the cost of introducing model mismatch.

Ignoring height, the state vector  $\mathbf{x}$  is thus composed of the East-North (EN) positions and EN velocities of each agent  $i = 1, \dots, M$  as  $x_i = [p_i, v_i]^\top$  where  $p_i, v_i \in \mathbb{R}^2$ . Similarly, the control  $\mathbf{u}$  consists of EN accelerations  $u_i \in \mathbb{R}^2$ . Eq. (1) decouples between the agents and takes the linear form

$$dx_i = Ax_i dt + B(u_i dt + d\xi_i),$$

$$A = \begin{bmatrix} 0 & 1 \\ 0 & 0 \end{bmatrix}, \quad B = \begin{bmatrix} 0 \\ 1 \end{bmatrix}. \quad (5)$$

Although the dynamics is decoupled and linear, the state cost  $r_t(\mathbf{x})$  in Eq. (2) is an arbitrary function of the joint space. As a result, the optimal control will in general be a non-linear function that couples all agents states.

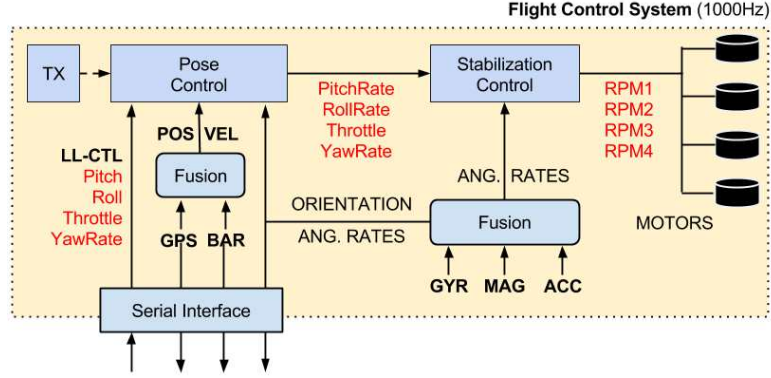


Figure 2: The flight control system (FCS) is comprised of two control loops: one for stabilization and the other for pose control. A low-level controller interacts with the FCS over a serial interface to stream measurements and issue control.

Given the current joint optimal action  $\mathbf{u}_t^*$  and velocity  $\mathbf{v}_t$ , the expected velocity at the next time  $t'$  is given by  $\mathbf{v}_{t'} = \mathbf{v}_t + (t' - t)\mathbf{u}_t^*$ . The expected velocity  $\mathbf{v}_{t'}$  together with a specified height  $h$ , are passed to the low-level controller, which is described next.

The final algorithm optionally keeps an importance-control sequence  $\mathbf{u}_{t:dt:t+H}$  that is incrementally updated. We summarize the algorithm as follows: at each control step, we measure the current state  $\mathbf{x}_t$  and perform the following steps:

---

**Algorithm 1** PI control for UAVs

---

- 1: **function** PICONROLLER( $N, H, dt, r_t(\mathbf{x}), \Sigma_u, \mathbf{u}_{t:dt:t+H}$ )
  - 2:   **for**  $k = 1, \dots, N$  **do**
  - 3:     Sample paths  $\tau_k = \{\mathbf{x}_{t:dt:t+H}\}_k$  with Eq. (5)
  - 4:   **end for**
  - 5:   Compute  $S_k = S(\tau_k | \mathbf{x}_0, \mathbf{u})$  with Eq. (2)
  - 6:   Store the noise realizations  $\{\xi_{t:dt:t+H}\}_k$
  - 7:   Compute the weights:  $w_k = e^{-S_k} / \sum_l e^{-S_l}$
  - 8:   **for**  $s = t : dt : t + H$  **do**
  - 9:      $\mathbf{u}_s^* = \mathbf{u}_s + \frac{1}{dt} \sum_k w_k (\{\xi_{s+dt}\}_k - \{\xi_s\}_k)$
  - 10:   **end for**
  - 11:   **Return** next desired velocity:  $\mathbf{v}_{t+dt} = \mathbf{v}_t + \mathbf{u}_t^* dt$  and optionally  $\mathbf{u}_{t:dt:t+H}^*$  for importance sampling at  $t + dt$
  - 12: **end function**
- 

The importance-control sequence  $\mathbf{u}_{t:dt:t+H}$  is typically initialized with zeros and noise is dimension-independent, i.e.  $\Sigma_u = \sigma_u^2 \text{Id}$ . To measure sampling convergence, we define the *Expected Sample Size* (ESS) as  $\text{ESS} := 1 / \sum_{k=1}^N w_k^2$ . Values of ESS close to one indicate an estimate dominated by just one sample and a poor estimate of the optimal control.

The target velocity  $\mathbf{v} = [v_E \ v_N]^T$  is passed along with a height  $\hat{p}_U$  to a VelocityHeight controller. The low-level controller uses the current state estimate of the real quadrotor  $\mathbf{y} = [p_E \ p_N \ p_U \ \phi \ \theta \ \psi \ u \ v \ w \ p \ q \ r]^T$ , where  $(p_E, p_N, p_U)$  and  $(\phi, \theta, \psi)$  denote navigation-frame position and orientation and  $(u, v, w), (p, q, r)$  denote body-frame and angular velocities, respectively. It is composed of four independent PID controllers for roll  $\hat{\phi}$ , pitch  $\hat{\theta}$ , throttle  $\hat{\gamma}$  and yaw rate  $\hat{r}$ . that send the commands to the flight control system (FCS) to achieve  $\mathbf{v}$ . Figure 2 shows the details of the FCS. The control loop runs at 1kHz, fusing angular velocity, linear acceleration and magnetic field strength measurements to estimate orientation and angular rates. The difference between the desired and actual angular rates are converted to motor speeds using the standard model [25].

An outer pose control loop calculates the desired angular rates based on the desired state. Orientation is obtained from the inner control loop, while position and velocity are obtained by fusing global posi-

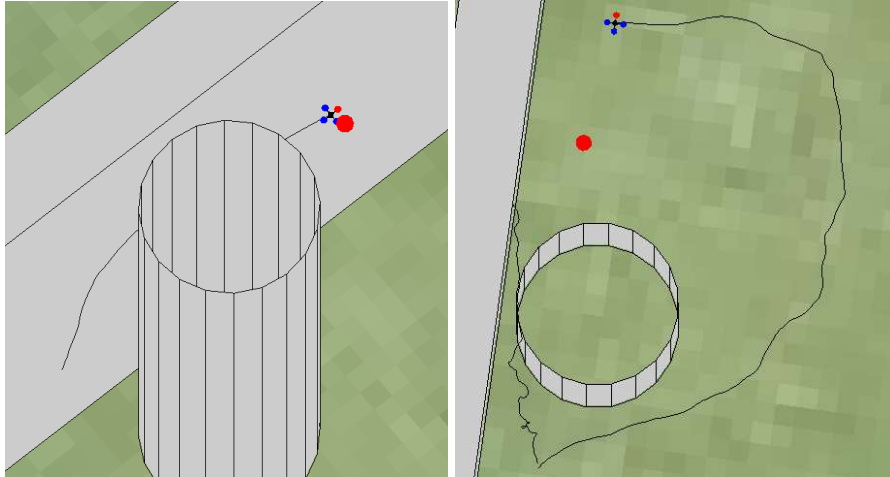


Figure 3: Drunken Quadrotor: a target (red spot) has to be reached while avoiding obstacles. (Left) the shortest route is the optimal solution in the absence of noise. (Right) with control noise, the optimal solution is to fly around the building.

tioning system (GPS) navigation fixes with barometric pressure (BAR) based altitude measurements. The radio transmitter (marked TX in the diagram) allows the operator to switch quickly between autonomous and manual control of a platform.

To simplify the testing and evaluation of the controllers, we developed an open-source framework, CRATES which is available online. The framework is an implementation of QRSim [26, 27] in Gazebo, which uses Robot Operating System (ROS) for high-level control. It permits high-level controllers, like Path Integral Control, to be platform-agnostic. It is similar to the Hector Quadrotor [28] project, with a formalized notion of a hardware abstraction layers.

The CRATES simulator propagates the quadrotor state forward in time based on a second order model [29]. The equations were learned from real flight data and verified by expert domain knowledge. In addition to platform dynamics, CRATES also simulates various noise-perturbed sensors, wind shear and turbulence. Orientation and barometric altitude errors follow zero-mean Ornstein-Uhlenbeck processes, while GPS error is modeled at the pseudorange level using trace data available from the International GPS Service. In accordance with the Military Specification MIL-F-8785C, wind shear is modelled as a function of altitude, while turbulence is modeled as a discrete implementation of the Dryden model. Finally, CRATES also provides support for generating terrain from satellite images and light detection and ranging (LIDAR) technology, and reporting collisions between platforms and terrain.

## 4 Results

We now analyze the proposed approach in three different tasks. We first show why in the presence of control noise, PI control is preferable over other approaches. For clarity, this scenario is presented for one agent only. We then consider the multi-agent setting in two tasks: a flight formation which requires coordinate of the UAVs and capturing a moving target that avoids the swarm.

We compare the PI control method described in Section 3.2 with iterative linear-quadratic Gaussian (iLQG) control [30], which iteratively computes local linear-quadratic approximations to the finite horizon problem. A key difference between iLQG and PI control is that the Linear-Quadratic approximation is certainty equivalent. Consequently, iLQG yields a noise independent solution.

### 4.1 Scenario I: Drunken Quadrotor

This scenario is inspired by [1] and highlights the benefits of SOC in the context of quadrotor control. The Drunken Quadrotor is a finite horizon task where a quadrotor has to reach a target, while avoiding a building and a wall (Figure 3). There are two possible routes: a shorter one that passes through a small

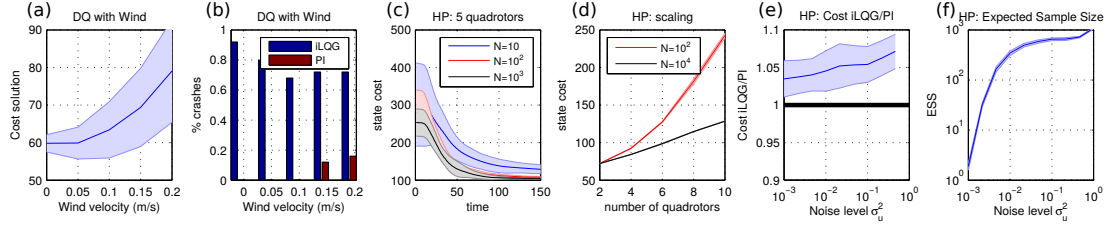


Figure 4: Results: **Drunken Quadrotor (DQ) with wind (a-b)**: For different wind velocities and fixed control noise  $\sigma_u^2 = 0.5$ , (a) cost of the obtained solutions and (b) percentage of crashes using iLQG and PI. **Holding pattern (HP) (c-f)**: (c) evolution of the state cost for different number of samples  $N = 10, 10^2, 10^3$ . (d) scaling of the method with the number of agents. For different control noise levels, (e) comparison between iLQG and PI control (ratios  $> 1$  indicate better performance of PI over iLQG) and (f) Expected Sample Sizes. Errors bars correspond to ten different random realizations.

gap between the wall and the building, and a longer one that goes around the building. Unlike SOC, the deterministic optimal solution does not depend on the noise level and will always take the shorter route. However, with added noise, the risk of collision increases and so the optimal noisy control is to take the longer route.

The state cost in this problem consists of hard constraints that assign infinite cost when either the wall or the building is hit. PI control deals with collisions by killing particles that hit the obstacles during Monte Carlo sampling. For iLQG, the local approximations require a twice differentiable cost function. We resolved this issue by adding asymptotes in the cost function. Although iLQG computes linear feedback, we tried to improve it with a MPC scheme, similar as for PI control. Unfortunately, this leads to numerical instabilities in this task, since the system disturbances tend to move the reference trajectory through a building when moving from one time step to the next. For MPC with PI control we use a receding horizon of three seconds and perform re-planning at a frequency of 15 Hz with  $N = 2000$  sample paths. Both methods are initialized with  $\mathbf{u}_t = 0, \forall t$ . iLQG requires approximately  $10^3$  iterations to converge with a learning rate of 0.5%.

Figure 3 (left) shows an example of real trajectory computed for low control noise level,  $\sigma_u^2 = 10^{-3}$ . To be able to obtain such a trajectory we deactivate sensor uncertainties in accelerometer, gyroscope, orientation and altimeter. External noise is thus limited to aerodynamic turbulences only. In this case, both iLQG and PI solutions correspond to the shortest path, i.e. go through the gap between the wall and the building. Figure 3 (right) illustrates the solutions obtained for larger noise level  $\sigma_u^2 = 1$ . While the optimal reference trajectory obtained by iLQG does not change, which results in collision once the real noisy controller is executed (left path), the PI control solution avoids the building and takes the longer route (right path).

We also consider more realistic conditions with noise not limited to act in the control. Figure 4 (a,b) shows results in the presence of wind and sensor uncertainty. Panel (a) shows how the wind affects the quality of the solution, resulting in an increase of the variance and the cost for stronger wind. In all our tests, iLQG was not able to bring the quadrotor to the other side. Panel (b) shows the percentage of crashes using both methods. Crashes occur very often using iLQG control and only occasionally using PI control. We conclude that for multi-modal tasks (tasks where multiple solution trajectories exist), the proposed method is preferable to iLQG.

## 4.2 Scenario II: Holding Pattern

The second scenario addresses the problem of coordinating agents to hold their position near a point of interest while keeping a safe range of velocities and avoiding crashing into each other. Such a problem arises for instance when multiple aircraft need to land at the same location, and simultaneous landing is not possible. The resulting flight formation is being used frequently in the literature [17, 9, 20, 31], but always with prior specification of the trajectories. We show how this formation is obtained as the optimal solution of a SOC problem.

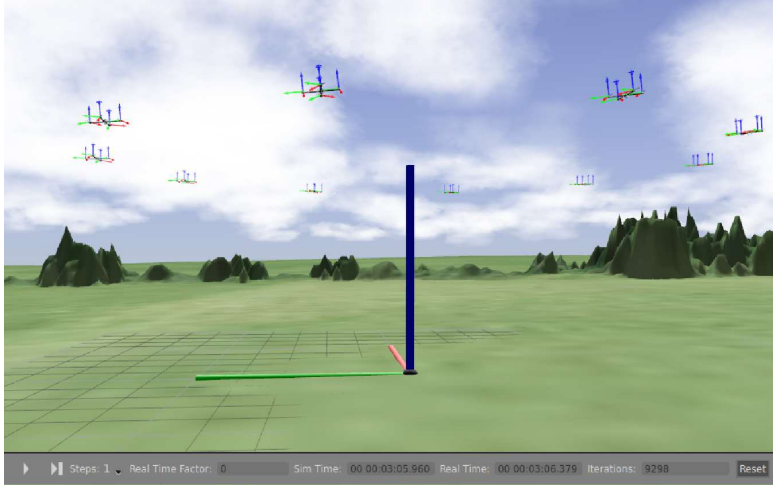


Figure 5: Holding pattern in the CRATES simulator. Ten quadrotors coordinate their flight in a circular formation. In this example,  $N = 10^4$  samples, control noise is  $\sigma_u^2 = 0.1$  and horizon  $H = 1$  sec. Cost parameters are  $v_{\min} = 1, v_{\max} = 3, C_{\text{hit}} = 20$  and  $d = 7$ . Environmental noise and sensing uncertainties are modeled using realistic parameter values.

Consider the following state cost (omitting time indexes)

$$r_{\text{HP}}(x) = \sum_{i=1}^M \exp(v_i - v_{\max}) + \exp(v_{\min} - v_i) + \exp(\|p_i - d\|_2) + \sum_{j>i}^M C_{\text{hit}} / \|p_i - p_j\|_2 \quad (6)$$

where  $v_{\max}$  and  $v_{\min}$  denote the maximum and minimum velocities, respectively,  $d$  denotes penalty for deviation from the origin and  $C_{\text{hit}}$  is the penalty for collision risk of two agents.  $\|\cdot\|_2$  denotes  $\ell_2$  norm.

The optimal solution for this problem is a circular flying pattern where units fly equidistantly from each other. The value of parameter  $d$  determines the radius and the average velocities of the agents are determined from  $v_{\min}$  and  $v_{\max}$ . Since the solution is symmetric with respect to the direction of rotation (clockwise or anti-clockwise), only when the control is executed, a choice is made and the symmetry is broken.

Figure 5 shows a snapshot of a simulation after the flight formation has been reached for a particular choice of parameter values.<sup>1</sup> Since we use an uninformed initial control trajectory, there is a transient period during which the agents organize to reach the optimal configuration. The coordinated circular pattern is obtained regardless of the initial positions. This behavior is robust and obtained for a large range of parameter values.

Figure 4(c) shows immediate costs at different times. Cost always decreases from the starting configuration until the optimal formation flight is reached. This value depends on several parameters. We report its dependence on the number  $N$  of sample paths. For large  $N$ , the variances are small and the cost attains small values. Conversely, for small  $N$ , there is larger variance and the obtained dynamical configuration is less optimal (typically the distances between the agents are not the same). During the formation of the pattern the controls are more expensive. For this particular task, full convergence of the path integrals is not required and the flight formation can be achieved with a very small  $N$ .

Figure 4(d) illustrates how the method scales as the number of agents increases. We report averages over the mean costs over 20 time-steps after one minute of flight. We varied  $M$  while fixing the rest of the parameters (the distance  $d$  which was set equal to the number of agents in meters). The small variance of the cost indicates that a stable formation is reached in all the cases. As expected, larger values of  $N$  lead to smaller state cost configurations.

Figure 4(e) shows how iLQG compares with PI control. Both use MPC, with a horizon of 2s and update frequency of 15Hz. We plot the ratio of cost differences after convergence of both solutions. Values above 1 indicate that PI control consistently outperforms iLQG in this problem. The Expected

<sup>1</sup>Supplementary video available at: <http://www.mbfys.ru.nl/staff/v.gomez/uav.html>

Sample Size (ESS) is shown in Figure 4(f) and illustrates the fact that higher control noise levels result in better exploration and thus better controls.

Figure 6 shows results obtained with the real platforms. (see the video that accompanies this paper for an experiment with three platforms). Despite the presence of significant noise in outdoors conditions, the circular behavior was also obtained. In the real experiments, we used a Core i7 laptop with 8GB RAM as base station, which run its own ROS messaging core and forwarded messages to and from the platforms over a IEEE 802.11 2.4GHz network. For safety reasons, the quadrotors were flown at different altitudes to avoid collisions. Summarizing, we have shown that the proposed PI control methodology is feasible and robust for coordinating a large swarm of quadrotors.

### 4.3 Scenario III: Cat and Mouse

The final scenario that we consider is the cat and mouse scenario. In this task, a team of  $M$  quadrotors (the cats) has to catch (get close to) another quadrotor (the mouse). The mouse has autonomous dynamics: it tries to escape the cats by moving at velocity inversely proportional to the distance to the cats. More precisely, let  $p_{\text{mouse}}$  denote the 2D position of the mouse, the velocity command for the mouse is computed (omitting time indexes) as

$$v_{\text{mouse}} = v_{\text{mouse}}^{\max} \frac{v}{\|v\|_2}, \quad \text{where } v = \sum_{i=1}^M \frac{p_i - p_{\text{mouse}}}{\|p_i - p_{\text{mouse}}\|_2}.$$

The parameter  $v_{\text{mouse}}^{\max}$  determines the maximum velocity of the mouse. As state cost function we use Eq. (6) with an additional penalty term that depends on the sum of the distances to the mouse

$$r_{\text{CM}}(x) = r_{\text{HP}}(x) + \sum_{i=1}^M \|p_i - p_{\text{mouse}}\|_2.$$

This scenario leads to several interesting dynamical states. For example, for a sufficiently large value of  $M$ , the mouse always gets caught (if its initial position is not close to the boundary, determined by  $d$ ). The optimal control for the cats is to surround the mouse to prevent collision. Once the mouse is surrounded, the cats keep rotating around it, as in the previous scenario, but with the origin replaced by the mouse position. For  $M = 2$  or a small time horizon, e.g.  $H = 1$ , the dynamical state in which the cats rotate around the mouse is not stable, and the mouse escapes. This is displayed in Figure 7 (bottom panels) and better illustrated in the video provided as supplementary material. We emphasize that these different behaviors are observed for large uncertainty in the form of sensor noise and wind. We can thus conclude that the proposed methodology allows for real-time control in highly complex scenarios.

## 5 Conclusions

This paper presents a centralized, real-time stochastic optimal control algorithm for coordinating the actions of multiple autonomous vehicles in order to minimize a global cost function. The high-level control task is expressed as a Path Integral control problem that can be solved using efficient sampling

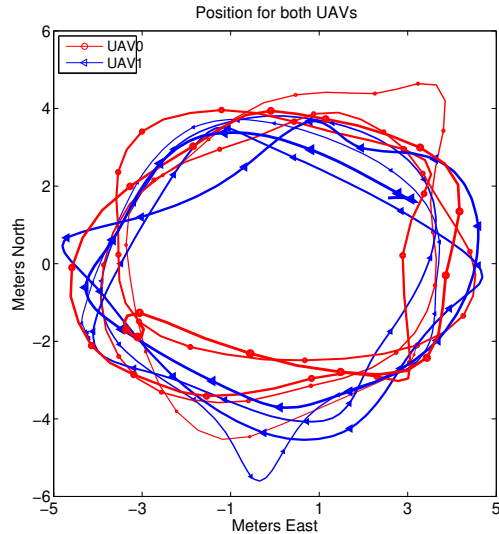


Figure 6: Resulting trajectories of a Holding Pattern experiment using two platforms in outdoors conditions.

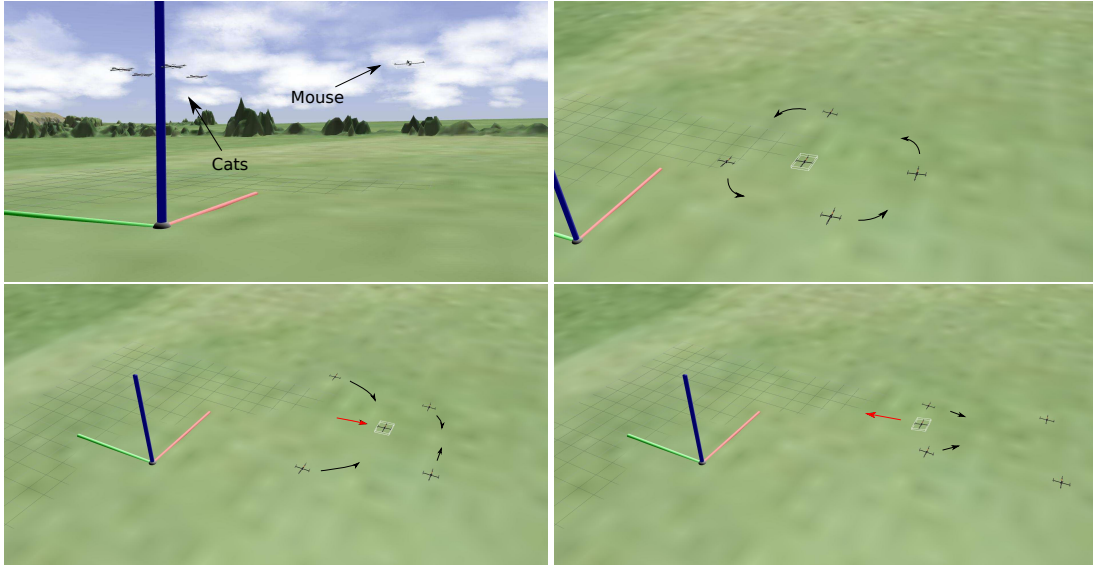


Figure 7: Cat and mouse scenario: **(Top-left)** four cats and one mouse. **(Top-right)** for horizon time  $H = 2$  seconds, the four cats surround the mouse forever and keep rotation around it. **(Bottom-left)** for horizon time  $H = 1$  seconds, the four cats chase the mouse but **(bottom-right)** the mouse manages to escape. With these settings, the multi-agent system alternates between these two dynamical states. Number of sample paths is  $N = 10^4$ , noise level  $\sigma_u^2 = 0.5$ . Other parameter values are  $d = 30$ ,  $v_{\min} = 1$ ,  $v_{\max} = 4$ ,  $v_{\min} = 4$  and  $v_{\max \text{ mouse}} = 3$ .

methods and real-time control is possible via the use of re-planning and model predictive control. To the best of our knowledge, this is the first real-time implementation of PI control on an actual multi-agent system.

We have shown in a simple scenario (Drunken Quadrotor) that the proposed methodology is more convenient than other approaches such as deterministic control or iLQG for planning trajectories. In more complex scenarios such as the Holding Pattern and Cat and Mouse, the proposed methodology is also preferable and allows for real-time control. We observe multiple and complex group behavior emerging from the specified cost function. Our experimental framework CRATES has been a key development that permitted a smooth transition from the theory to the real quadrotor platforms, with literally no modification of the underlying control code. This gives evidence that the model mismatch caused by the use of simplified, double integrator dynamics is not critical in normal outdoor conditions. Our current research is addressing the following aspects:

**Large scale parallel sampling**— the embarrassingly parallel nature of PI control makes it amenable for parallelization, for instance, using graphics processing units. Although the tasks considered in this work did not required more than  $10^4$  samples, we expect that this improvement will significantly increase the number of application domains.

**Distributed control**— we are exploring different distributed formulations that take better profit of the factorized representation of the state cost. Note he that the costs functions considered in this work only require pairwise couplings of the agents (to prevent collisions). However, full observability of the joint space is still required, which is not available in a fully distributed approach.

## References

- [1] H. J. Kappen, “Path integrals and symmetry breaking for optimal control theory,” *Journal of statistical mechanics: theory and experiment*, vol. 2005, no. 11, p. P11011, 2005.
- [2] F. Kendoul, “Survey of advances in guidance, navigation, and control of unmanned rotorcraft systems,” *J. Field Robot.*, vol. 29, no. 2, pp. 315–378, 2012.

- [3] E. Todorov, “Linearly-solvable Markov decision problems,” in *Advances in Neural Information Processing Systems 19*, 2006, pp. 1369–1376.
- [4] K. Kinjo, E. Uchibe, and K. Doya, “Evaluation of linearly solvable Markov decision process with dynamic model learning in a mobile robot navigation task,” *Front. Neurobot.*, vol. 7, pp. 1–13, 2013.
- [5] E. Rombokas, E. Theodorou, M. Malhotra, E. Todorov, and Y. Matsuoka, “Tendon-driven control of biomechanical and robotic systems: A path integral reinforcement learning approach,” in *International Conference on Robotics and Automation (ICRA)*, 2012, pp. 208–214.
- [6] E. Theodorou, J. Buchli, and S. Schaal, “A generalized path integral control approach to reinforcement learning,” *J. Mach. Learn. Res.*, vol. 11, pp. 3137–3181, 2010.
- [7] H. J. Kappen, V. Gómez, and M. Opper, “Optimal control as a graphical model inference problem,” *Mach. Learn.*, vol. 87, pp. 159–182, 2012.
- [8] B. Van Den Broek, W. Wiegerinck, and H. J. Kappen, “Graphical model inference in optimal control of stochastic multi-agent systems,” *J. Artif. Intell. Res.*, vol. 32, pp. 95–122, 2008.
- [9] J. How, B. Bethke, A. Frank, D. Dale, and J. Vian, “Real-time indoor autonomous vehicle test environment,” *IEEE Contr. Syst. Mag.*, vol. 28, no. 2, pp. 51–64, 2008.
- [10] G. M. Hoffmann, H. Huang, S. L. Waslander, and C. J. Tomlin, “Precision flight control for a multi-vehicle quadrotor helicopter testbed,” *Control. Eng. Pract.*, vol. 19, no. 9, pp. 1023 – 1036, 2011.
- [11] D. H. Shim, H. J. Kim, and S. Sastry, “Decentralized nonlinear model predictive control of multiple flying robots,” in *IEEE conference on Decision and control (CDC)*, vol. 4, 2003, pp. 3621–3626.
- [12] A. Kushleyev, D. Mellinger, C. Powers, and V. Kumar, “Towards a swarm of agile micro quadrotors,” *Auton. Robot.*, vol. 35, no. 4, pp. 287–300, 2013. [Online]. Available: <http://dx.doi.org/10.1007/s10514-013-9349-9>
- [13] M. Turpin, N. Michael, and V. Kumar, “Decentralized formation control with variable shapes for aerial robots,” in *International Conference on Robotics and Automation (ICRA)*, 2012, pp. 23–30.
- [14] F. Augugliaro, A. Schoellig, and R. D’Andrea, “Generation of collision-free trajectories for a quadcopter fleet: A sequential convex programming approach,” in *Intelligent Robots and Systems (IROS)*, 2012, pp. 1917–1922.
- [15] C. W. Reynolds, “Flocks, herds and schools: A distributed behavioral model,” *SIGGRAPH Comput. Graph.*, vol. 21, no. 4, pp. 25–34, 1987.
- [16] J. Guerrero and R. Lozano, *Flight Formation Control*. John Wiley & Sons, 2012.
- [17] G. Vásárhelyi, C. Virágh, G. Somorjai, N. Tarcai, T. Szörényi, T. Nepusz, and T. Vicsek, “Outdoor flocking and formation flight with autonomous aerial robots,” in *Intelligent Robots and Systems (IROS)*, 2014.
- [18] S. Hauert, S. Leven, M. Varga, F. Ruini, A. Cangelosi, J.-C. Zufferey, and D. Floreano, “Reynolds flocking in reality with fixed-wing robots: Communication range vs. maximum turning rate,” in *Intelligent Robots and Systems (IROS)*, 2011, pp. 5015–5020.
- [19] A. Bürkle, F. Segor, and M. Kollmann, “Towards autonomous micro UAV swarms,” *J. Intell. Robot. Syst.*, vol. 61, no. 1-4, pp. 339–353, 2011.
- [20] B. Yu, X. Dong, Z. Shi, and Y. Zhong, “Formation control for quadrotor swarm systems: Algorithms and experiments,” in *Chinese Control Conference (CCC)*, 2013, pp. 7099–7104.

- [21] S. Quintero, G. Collins, and J. Hespanha, “Flocking with fixed-wing UAVs for distributed sensing: A stochastic optimal control approach,” in *American Control Conference (ACC)*, 2013, pp. 2025–2031.
- [22] S. Thijssen and H. J. Kappen, “Path integral control and state dependent feedback,” *Physical Review E*, 2014, ”in press”.
- [23] M. B. Horowitz, A. Damle, and J. W. Burdick, “Linear Hamilton Jacobi Bellman equations in high dimensions,” *arXiv preprint arXiv:1404.1089*, 2014.
- [24] V. Gómez, H. J. Kappen, J. Peters, and G. Neumann, “Policy search for path integral control,” in *European Conference on Machine Learning and Principles and Practice of Knowledge Discovery in Databases (ECML/PKDD)*, 2014, vol. 8724, pp. 482–497.
- [25] R. Mahony, V. Kumar, and P. Corke, “Multirotor aerial vehicles: Modeling, estimation, and control of quadrotor,” *IEEE Robotics & Automation Magazine*, pp. 20–32, Sept. 2012. [Online]. Available: [http://ieeexplore.ieee.org/xpls/abs\\_all.jsp?arnumber=6289431](http://ieeexplore.ieee.org/xpls/abs_all.jsp?arnumber=6289431)
- [26] R. De Nardi, “The QRSim Quadrotors Simulator,” Department of Computer Science, University College London, Tech. Rep. RN/13/08, March 2013.
- [27] A. C. Symington, R. de Nardi, S. J. Julier, and S. Hailes, “Simulating quadrotor UAVs in outdoor scenarios,” in *Intelligent Robots and Systems (IROS)*, 2014.
- [28] J. Meyer, A. Sendobry, S. Kohlbrecher, and U. Klingauf, “Comprehensive Simulation of Quadrotor UAVs Using ROS and Gazebo,” *Lecture Notes in Computer Science*, vol. 7628, pp. 400–411, 2012.
- [29] R. De Nardi and O. Holland, “Coevolutionary modelling of a miniature rotorcraft,” in *10th International Conference on Intelligent Autonomous Systems (IASIO)*, 2008, pp. 364 – 373.
- [30] E. Todorov and W. Li, “A generalized iterative LQG method for locally-optimal feedback control of constrained nonlinear stochastic systems,” in *American Control Conference, 2005. Proceedings of the 2005.* IEEE, June 2005, pp. 300–306 vol. 1.
- [31] A. Franchi, C. Masone, V. Grabe, M. Ryll, H. H. Bühlhoff, and P. R. Giordano, “Modeling and control of UAV bearing-formations with bilateral high-level steering,” *Int. J. Robot. Res.*, p. 0278364912462493, 2012.